Transit-time effects in coherent transient spectroscopy

J. L. Cohen [1] and P. R. Berman [2]
[1] *Applied Physics Program, Department of Physics, University of Michigan, Ann Arbor, Michigan 48109-1120*
[2] *Department of Physics, University of Michigan, Ann Arbor, Michigan 48109-1120*
(Received 30 May 1996)

We have developed a general technique for obtaining analytical expressions for coherent transient signals arising from atoms interacting with two or more laser pulses having Gaussian spatial profiles. After deriving the Maxwell-Bloch equations for short laser pulses incident on an ensemble of three-level atoms, we specialize to photon echo spectroscopy. As an example, the stimulated photon echo signal is calculated as a function of the time delay between pulses. Our exact results are compared with both the lowest-order perturbative limit and a calculation in which transit time is treated phenomenologically. We conclude by commenting on the extension of our technique to atoms undergoing velocity-changing collisions. [S1050-2947(96)07011-4]

PACS number(s): 42.50.Md, 42.50.Hz, 42.62.Fi, 42.65.Vh

I. INTRODUCTION

Optical coherent transients have been used extensively for high-precision atomic and molecular spectroscopy and to probe the relaxation processes of quantum coherences and populations due to radiative and collisional broadening [1]. In one class of photon echo experiments, several traveling-wave (TW) and/or standing-wave (SW) pulses are incident on a thermal vapor, and the radiation from the coherent atomic response is observed at a later time [1–7]. The basic photon echo is produced when two laser pulses, separated by a time T, interact with a sample [1,2,8]. The first pulse creates a coherence between the atomic states, which undergoes Doppler dephasing in a time $(\mathbf{k}u)^{-1}$, where $\mathbf{k}$ is the laser wave vector and u is the most probable atomic speed. At time T, this dephasing is reversed by the second laser pulse, and the atomic dipoles rephase and radiate at time $2T$. As a function of T, this echo signal decays exponentially at the radiative rate γ, constraining the duration time of an experiment to time separations $T<(2\gamma)^{-1}$ and limiting the basic echo's usefulness as a probe of weak velocity-changing collisions.

The time constraint can be overcome by using a stimulated photon echo (SE), involving three copropagating TW pulses, and by using other echo schemes that probe the modulated population of long-lived, ground-state magnetic sublevels. Such experiments can be used to study collisions between active and perturber atoms in different pressure regimes [5,6]. Due to advances in the stability and tunability of pulsed laser sources, new echo experiments on longer time scales are now achievable. Yet, in atomic experiments that occur over time scales on the order of the average transit time through the laser beam, the center-of-mass motion across the transverse intensity profile must be accounted for theoretically in order to interpret the data [9]. Typically, some effective, homogeneous rate γ_{tr} has been used to model motion out of the experimental region, where the transit rate γ_{tr} is defined as u divided by the laser beam width. The correct approach, however, includes the transverse laser profile directly in the atom-field coupling.

Previously, several authors have broached this subject for both frequency-domain [10,11] and time-domain [12,13] spectroscopy. In the time domain, transverse transit effects have, to our knowledge, been introduced only in perturbation theory. Since nonperturbative, analytic density matrix calculations can be performed for photon echoes in the short-pulse limit for each velocity subclass, and since this is the most important experimental regime (i.e., echoes induced by short π and $\pi/2$ pulses, etc.), we present a general theoretical technique that properly accounts for transit-time effects in Gaussian laser beams caused by classical center-of-mass motion. The significant result of this paper is as follows. For echo experiments where velocity-changing collisions are negligible, the off-diagonal density matrix elements responsible for a macroscopic polarization can be expressed as a product of analytic functions of the laser pulse areas multiplied by the transverse-field profile. These functions can then be expanded in power series and integrated analytically in Cartesian coordinates over the Maxwellian velocity distribution and over the transverse coordinates. This yields a final result for the detected signal pulse in terms of a rapidly converging sum over the expansion indices, where each term in the sum can be linked to a specific order in perturbation theory.

In Sec. II, we write down the equations of motion for the density matrix of ''open'' three-level atoms coupled to a sequence of laser pulses. The echo signal is then derived from the Maxwell-Bloch equations in the slowly varying envelope (SVEA) and thin-medium approximations. We consider a measurement of the total echo pulse energy as a function of the various time delays between laser pulses for transit times which are long compared to the Doppler dephasing time. A corresponding expression for heterodyne detection is given as well. In Sec. III, two calculations of experimental interest are presented. First, the SE signal is found for typical laboratory conditions. The decay of the signal as a function of the time between the second and third laser pulses is shown to be slower for strong pulses when compared to weak excitation. Second, the signal for the grating stimulated echo (GSE) is discussed [5,6], where two TW laser pulses, a SW pulse, and a TW pulse are applied to a vapor, which subsequently radiates a TW pulse. The GSE is more sensitive to velocity-changing collisions than the SE and can be used to measure the detailed form of the collision

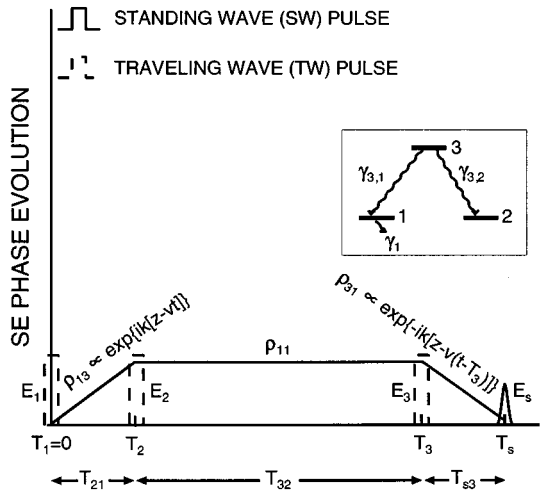

FIG. 1. Doppler phase diagram for the stimulated photon echo (SE). The phase of the density-matrix elements that contributes to a SE signal is shown for one velocity subclass. The ground-state population ρ_{11} evolves without a Doppler (velocity-dependent) phase for a time T_{32}. The important transit regime for the SE occurs for T_{32} on the order of the average atomic travel time through the Gaussian transverse distribution of the laser pulses. The inset shows the three-level model used here, where the laser pulses resonantly couple states 1 and 3 only. Spontaneous emission from level 3 to level 2 opens the system, allowing for SE experiments involving long-lived ground states such as level 1.

kernel. In Sec. IV, we conclude by commenting on the extension of our approach to the collision regime. In Appendix A, we show the general form of any photon echo signal that fits within our model. In Appendix B, a transit-time decay function for the SE signal is derived in detail by performing the necessary transverse velocity and coordinate integrations.

II. MAXWELL-BLOCH EQUATIONS IN PULSED LASER FIELDS AND THE ECHO SIGNAL

A gas of three-level atoms (Fig. 1, inset) in a vapor cell of length L interacts with a series of N laser pulses. This is the same model as that adopted in Refs. [5–7]. Only levels 1 and 3, separated in energy by $\hbar\omega$, are driven by the field. Level 1 is a ground-state sublevel, assigned a decay rate γ_1 for generality. For our calculations we are interested in the limit $\gamma_1 \rightarrow 0$, since we take into account transverse motion explicitly. We can then compare our result with a phenomenological model in which $\gamma_1 \neq 0$ and the transverse spatial dependence of the laser field is neglected. Level 2 is an all-purpose level, which simply represents another decay channel for level 3 and thereby opens the system [6]. Level 3 decays spontaneously to levels 1 and 2 with rates $\gamma_{3,1}$ and $\gamma_{3,2}$, respectively. For this system, the ground-state lifetime γ_1^{-1} is the longest time scale and, in particular, $\gamma_1 \ll \gamma_{3,1}, \gamma_{3,2}$.

We consider pulse propagation only along the z axis, so that the transverse coordinates are defined as x and y. The laser pulses, each with central frequency Ω, can be written as a radiation field

$$\mathbf{E}(x,y,z,t) = \frac{1}{2} e^{-i\Omega t} \hat{\boldsymbol{\epsilon}} \sum_{j=1}^{N} E_j U_j(z) \times \exp\left[-\left(\frac{x^2}{x_j^2} + \frac{y^2}{y_j^2} \right) \right] f_j\left(\frac{t - T_j}{\tau_j} \right) + \text{c.c.}, \quad (1)$$

where $\hat{\boldsymbol{\epsilon}}$ is the polarization of the field, E_j and $k_j = \pm k$ ($k \equiv \Omega/c$) are the amplitude and propagation vector of the jth pulse, and

$$U_j(z) = \begin{cases} e^{ik_j z} & \text{for TW pulses} \\ \cos k_j z & \text{for SW pulses.} \end{cases} \quad (2)$$

(For geometries where echoes are created by pulses at small angles with respect to each other, $U_j(z)$ can be generalized to $U_j(\mathbf{k}_j \cdot \mathbf{R})$ for $\mathbf{k}_j \approx k_j \hat{z} + (\delta k)_j \hat{x}$, as in Ref. [6].) The transverse profile in Eq. (1) is taken as a product of real Gaussians with widths x_j and y_j for the x and y directions, respectively. We can therefore account for elliptical intensity distributions. The temporal pulse envelopes $f_j(t)$, centered at times T_j, have pulse widths τ_j. Each pulse has a spatial extent larger than the vapor cell, $c\tau_j > L \gg \lambda$, allowing us to use a thin-medium approximation. Pulses are applied sequentially so that $T_j < T_i$ for $j < i$. The time between pulses is

$$T_{ij} = T_i - T_j, \quad (3)$$

and the signal is observed at $t = T_s$.

The following general assumptions are made about the experimental conditions. The atoms are assumed to travel in straight, classical paths, $\mathbf{R}(t) = \mathbf{R}_0 + \mathbf{v}t$. Motion along the laser propagation direction leads to a Doppler shift, while motion in the radial direction modifies the strength of the atom-field interaction at the different T_j's, owing to the transverse-laser profile. The pulses are considered short compared to all other dynamical time scales in the problem, so that both decay and atomic motion can be neglected while each pulse acts. Furthermore, the pulses are well separated in time ($\tau_i \ll T_{ij}$ for all $i > j$). Therefore, calculations are performed by dividing the problem into two different types of time regions: (i) regions where the pulsed fields act and (ii) field-free regions between pulses where relaxation and atomic motion occur. In addition, collisions are included only as a homogeneous dephasing mechanism for the off-diagonal density matrix; for the diagonal elements, velocity-changing collisions are neglected in our calculations but discussed in the Conclusion, Sec. IV. For the only previous calculation of photon echo transit effects, Thomas and Forber in Ref. [13] use the same considerations. We modify and extend their result beyond the perturbative, two-pulse regime. Other specific conditions depend on the echo process considered and will be stated in Sec. III for the SE and the GSE separately.

The density-matrix master equations are written in a field-interaction representation defined by

$$\rho_{31} = \rho_{13}^* = \tilde{\rho}_{31} e^{-i\Omega t}. \quad (4)$$

The population of level 2, ρ_{22}, does not participate in the coherent dynamics and will not be considered further. The

coherences, ρ_{21} and ρ_{32}, are zero initially and therefore remain zero for all time. The remaining equations for the effective two-level atom are

$$\frac{d}{dt}\rho_{11}=-\gamma_1\rho_{11}+\gamma_{3,1}\rho_{33}+\left(-i\sum_{j=1}^{N}\chi_j f_j\left(\frac{t-T_j}{\tau_j}\right)U_j^*(z)\times\exp\left[-\left(\frac{x_{T_j}^2}{x_j^2}+\frac{y_{T_j}^2}{y_j^2}\right)\right]\widetilde{\rho}_{31}+\text{c.c.}\right), \tag{5a}$$

$$\frac{d}{dt}\rho_{33}=-(\gamma_{3,1}+\gamma_{3,2})\rho_{33}+\left(i\sum_{j=1}^{N}\chi_j f_j\left(\frac{t-T_j}{\tau_j}\right)U_j^*(z)\times\exp\left[-\left(\frac{x_{T_j}^2}{x_j^2}+\frac{y_{T_j}^2}{y_j^2}\right)\right]\widetilde{\rho}_{31}+\text{c.c.}\right), \tag{5b}$$

$$\frac{d}{dt}\widetilde{\rho}_{31}=-(\gamma+i\delta)\widetilde{\rho}_{31}+i\sum_{j=1}^{N}\chi_j f_j\left(\frac{t-T_j}{\tau_j}\right)U_j(z)\times\exp\left[-\left(\frac{x_{T_j}^2}{x_j^2}+\frac{y_{T_j}^2}{y_j^2}\right)\right](\rho_{33}-\rho_{11}), \tag{5c}$$

where the atom-field interaction Hamiltonian is $-\mathbf{d}\cdot\mathbf{E}$, $\mathbf{d}$ is the atomic-dipole-moment operator, $d/dt\equiv(\partial/\partial t)+v_z(\partial/\partial z)$ is a convective derivative, and v_z is the z component of the velocity. Clearly, the density operator depends on time, position, and atomic velocity, $\rho=\rho(t=T_s,\mathbf{R}(t),\mathbf{v})$. Atomic recoil and gradient forces on the atoms have been neglected.

The Rabi frequency for the peak of the jth pulse,

$$\chi_j=-\frac{dE_j}{2\hbar}, \tag{6}$$

is taken as real in Eqs. (5a)–(5c), where d is the dipole-matrix element $\langle 3|\mathbf{d}\cdot\hat{\boldsymbol{\epsilon}}|1\rangle$. For an individual atom, the phase and strength of the jth pulse are determined by the atomic position at T_j relative to the observation position at time T_s,

$$\mathbf{R}(T_j)=\mathbf{R}(t=T_s)-\mathbf{v}T_{sj}\Leftrightarrow\begin{pmatrix}x_{T_j}\\y_{T_j}\\z_{T_j}\end{pmatrix}=\begin{pmatrix}x\\y\\z\end{pmatrix}-\begin{pmatrix}v_x\\v_y\\v_z\end{pmatrix}T_{sj}. \tag{7}$$

This corresponds to calculations done in the fixed-coordinate system of the laboratory rest frame, where the convective derivative accounts for motion along the z axis. In Eq. (5c) the atomic dipole decays at the rate $\gamma\approx[(\gamma_{3,2}+\gamma_{3,1})/2]+\Gamma$ for the homogeneous collision rate Γ.

Equations (5a)–(5c) are a generalized form of the optical Bloch equations. We set the atom-field detuning $\delta=\omega-\Omega=0$ in (5c), on the assumption that $\tau_j|\delta|,\tau_j|k_j|u\ll 1$. When the field acts at T_j, the density matrix immediately following the pulse $\rho(T_j^+)$ is expressed in terms of the matrix preceding the pulse $\rho(T_j^-)$ as [6,14]

$$\rho_{11}(T_j^+)=\frac{1}{2}\{1+\cos[\alpha_j(z)\Theta_j]\}\rho_{11}(T_j^-)+\frac{1}{2}\{1-\cos[\alpha_j(z)\Theta_j]\}\rho_{33}(T_j^-)-\left\{\frac{i}{2}\sin[\alpha_j(z)\Theta_j]\beta_j^*(z)\widetilde{\rho}_{31}(T_j^-)+\text{c.c.}\right\}, \tag{8a}$$

$$\rho_{33}(T_j^+)=\frac{1}{2}\{1-\cos[\alpha_j(z)\Theta_j]\}\rho_{11}(T_j^-)+\frac{1}{2}\{1+\cos[\alpha_j(z)\Theta_j]\}\rho_{33}(T_j^-)+\left\{\frac{i}{2}\sin[\alpha_j(z)\Theta_j]\beta_j^*(z)\widetilde{\rho}_{31}(T_j^-)+\text{c.c.}\right\}, \tag{8b}$$

$$\widetilde{\rho}_{31}(T_j^+)=-\frac{i}{2}\sin[\alpha_j(z)\Theta_j]\beta_j(z)\rho_{11}(T_j^-)+\frac{i}{2}\sin[\alpha_j(z)\Theta_j]\beta_j(z)\rho_{33}(T_j^-)+\frac{1}{2}\{1+\cos[\alpha_j(z)\Theta_j]\}\widetilde{\rho}_{31}(T_j^-)+\frac{1}{2}\{1-\cos[\alpha_j(z)\Theta_j]\}\widetilde{\rho}_{13}(T_j^-)[\beta_j(z)]^2, \tag{8c}$$

$$\widetilde{\rho}_{13}(T_j^+)=\widetilde{\rho}_{31}^*(T_j^+). \tag{8d}$$

The effective pulse area is defined as the usual pulse area multiplied by a transverse position function,

$$\Theta_j=\{\theta_j\}\times H_j(x,y,v_x,v_y)=\left\{2\chi_j\int_{-\infty}^{+\infty}f_j\left(\frac{t}{\tau_j}\right)dt\right\}\times\exp\left[-\left(\frac{x-v_xT_{sj}}{x_j}\right)^2-\left(\frac{y-v_yT_{sj}}{y_j}\right)^2\right], \tag{9}$$

and the spatial modulation factors are

$$\alpha_j(z)=\begin{cases}1\text{ for TW pulses}\\\cos k_j z\ \text{ for SW pulses}\end{cases}$$

and

$$\beta_j(z)=\begin{cases}e^{ik_jz}\ \text{ for TW pulses}\\1\ \text{ for SW pulses.}\end{cases} \tag{10}$$

In Eq. (9), we see immediately that the transverse profile creates a spatially dependent atom-field interaction strength.

For the time intervals between pulses j and $i=j+1$, the optical Bloch equations (5a)–(5c) give

$$\rho_{11}(T_i^-)=\left\{\rho_{11}(T_j^+)e^{-\gamma_1 T_{ij}}+\rho_{33}(T_j^+)\frac{\gamma_{3,1}}{\gamma_{3,1}+\gamma_{3,2}-\gamma_1}\times[e^{-\gamma_1 T_{ij}}-e^{-(\gamma_{3,1}+\gamma_{3,2})T_{ij}}]\right\}\times\exp[-iK_j^{(11)}v_z T_{ij}], \tag{11a}$$

$$\rho_{33}(T_i^-)=\rho_{33}(T_j^+)e^{-(\gamma_{3,1}+\gamma_{3,2})T_{ij}}\exp[-iK_j^{(33)}v_z T_{ij}], \tag{11b}$$

$$\tilde{\rho}_{31}(T_i^-)=\tilde{\rho}_{31}(T_j^+)e^{-\gamma T_{ij}}\exp[-iK_j^{(31)}v_z T_{ij}], \tag{11c}$$

$$\tilde{\rho}_{13}(T_i^-)=\tilde{\rho}_{31}^*(T_i^-). \tag{11d}$$

In Eqs. (11a)–(11d), the velocity-dependent phases are defined formally using

$$K_j^{(ab)}=\frac{\partial\rho_{ab}(T_j^+)}{\partial z}\frac{1}{i\rho_{ab}(T_j^+)}, \tag{12}$$

allowing atomic-state populations to be modulated by counterpropagating fields. When a time interval is long, so that $(\gamma_{3,1}+\gamma_{3,2})^{-1}\ll T_{ij}\ll\gamma_1^{-1}$, the upper-state population $\rho_{33}(T_i^-)$ and coherence $\tilde{\rho}_{31}(T_i^-)$ decay, while for $\gamma_{3,2}\neq 0$ a modulated ground-state population $\rho_{11}(T_i^-)$ remains. For the Fourier components of the density matrix that contribute to an echo, $\rho_{11}(T_j^+)=-\rho_{33}(T_j^+)$, implying from Eq. (11a) that $\rho_{11}(T_{j+1}^-)\propto\rho_{11}(T_j^+)[(\gamma_{3,2})/(\gamma_{3,1}+\gamma_{3,2})]$. These conditions show that echo signals on long time scales are only possible for an open two-level system which includes a decay channel such as level 2, $\gamma_{3,2}\gg\gamma_1\geq 0$. Both the SE and the GSE that we consider in Sec. III exhibit this behavior.

To describe a signal field generated by the atomic dipoles, the electric field and polarization vectors are decomposed into Fourier components with slowly varying envelopes,

$$\begin{pmatrix}\mathbf{E}_s\\ \mathbf{P}_s\end{pmatrix}=\frac{1}{2}\hat{\boldsymbol{\epsilon}}\begin{pmatrix}E_s(x,y,t)\\ P_s(x,y,t)\end{pmatrix}e^{ik_s z-i\Omega t}+\text{c.c.} \tag{13}$$

Phase matching requires that $k_s=\pm k$. When inserted into the Maxwell equations, the signal field can be related directly to the polarization envelope in the SVEA for a thin medium,

$$E_s=\frac{ik_s L}{2\epsilon_0}P_s. \tag{14}$$

The macroscopic polarization is defined as the total dipole moment density averaged over the inhomogeneous velocity distribution,

$$P_s=2nd\int d\mathbf{v}\tilde{\rho}_{31}(t,x,y,z,\mathbf{v})e^{-ik_s z}, \tag{15}$$

for the atomic density n. Momentum conservation determines which spatial Fourier components of $\tilde{\rho}_{31}(t,x,y,z,\mathbf{v})$ can radiate, restricting k_s in Eqs. (14) and (15) to those values for which the spatial phase of P_s vanishes, where we assume that the signal is a TW pulse. Standing-wave echo pulses can be treated in a similar manner [3]. These coupled Maxwell-Bloch equations (8)–(15) for short pulses can be used to study optical coherent transients in general.

A general solution for photon echo signals at $T_s > T_N$ for $T_1=0$ is derived in Appendix A for the initial conditions,

$$\rho_{33}(t=0^-)=\rho_{31}(t=0^-)=0,$$
$$\rho_{11}(t=0^-)=W_0(\mathbf{v}), \tag{16}$$

where $W_0(\mathbf{v})=(\pi u^2)^{-3/2}e^{-|\mathbf{v}|^2/u^2}$ is the Maxwellian velocity distribution. We define the detectable echo signal as the total energy of the radiated echo field,

$$S=\int dT_s\int\int dx\,dy\,\frac{1}{2}\epsilon_0 c|E_s|^2. \tag{17}$$

[For heterodyne detection, $E_s(x,y,t)$ is combined with a strong field $E_0(x,y,t)$ at the same frequency, and the signal, subtracting out a constant background, is proportional to $\int dT_s\int\int dx\,dy\,\mathrm{Re}\{E_0^*(x,y,T_s)E_s(x,y,T_s)\}$.] Combining Eqs. (14), (15), and (17), the final signal expression is rewritten as

$$S=\frac{(k_s Lnd)^2 c}{2\epsilon_0}\times\int dT_s\int\int dx\,dy\left|\int d\mathbf{v}\tilde{\rho}_{31}(T_s,x,y,z,\mathbf{v})e^{-ik_s z}\right|^2. \tag{18}$$

III. ECHO CALCULATIONS IN THE TRANSIT REGIME

A. The stimulated-echo signal

Stimulated echo experiments follow the Doppler phase diagram of Fig. 1. The three excitation pulses are all TW fields propagating in the $+z$ direction, $k_1=k_2=k_3=k_s=k$. The first pulse creates a coherence $\tilde{\rho}_{13}(T_1^+)$, which dephases in a time $(ku)^{-1}$. The time to the second pulse T_{21} is chosen such that $(ku)^{-1}<T_{21}$. The second pulse ''stops'' the Doppler dephasing by creating a component of the ground-state population $\rho_{11}(T_2^+)$ that varies as $e^{i(k_2-k_1)z}$. This component evolves over time T_{32} with a velocity-independent phase. For $(\gamma_{3,1}+\gamma_{3,2})^{-1}\ll T_{32}\ll\gamma_1^{-1}$, T_{32} is a long time period, as discussed after Eq. (12) — any coherence or excited-state population has decayed completely by the time the third pulse acts on the modulated ground state. This third pulse reverses the Doppler dephasing of the dipole $\tilde{\rho}_{31}$ that occurred between the first and second pulses, leading to SE radiation peaked at the time $T_s=T_3+T_{21}$.

Solving Eqs. (8a)–(8d) and (11a)–(11d) in this scheme for $\tilde{\rho}_{31}(T_s,x,y,z,\mathbf{v})$ with the initial conditions of Eq. (16), we find

$$\tilde{\rho}_{31}(T_s,x,y,z,\mathbf{v})=-\frac{i}{8}W_0(\mathbf{v})\frac{\gamma_{3,2}}{\gamma_{3,1}+\gamma_{3,2}}e^{-\gamma_1 T_{32}}\times e^{-\gamma(T_s-T_3+T_{21})}e^{-ikv_z(T_s-T_3-T_{21})}\times\sin\Theta_1\sin\Theta_2\sin\Theta_3 e^{ikz}, \tag{19}$$

where Θ_j is given by Eq. (9). Substituting this expression into Eq. (18) and integrating over v_z gives the SE signal,

$$S_{SE}=\frac{(k_sLnd)^2c}{128\epsilon_0}\left(\frac{\gamma_{3,2}}{\gamma_{3,1}+\gamma_{3,2}}\right)^2\int dT_s e^{-1/2[ku(T_s-T_3-T_{21})]^2}\times e^{-2\gamma_1 T_{32}}e^{-2\gamma(T_s-T_3+T_{21})}B(T_s). \quad (20)$$

The echo intensity is sharply peaked at the rephasing time $T_s=T_3+T_{21}$, as it should be. The quantity $B(T_s)$ represents the transverse polarization effects which are the central result of this paper,

$$B(T_s)=\int\int dxdy\left|\int\int\frac{dv_xdv_y}{\pi u^2}e^{-(v_x^2+v_y^2)/u^2}\times\sin\Theta_1\sin\Theta_2\sin\Theta_3\right|^2. \quad (21)$$

It varies slowly in time compared to the Gaussian in Eq. (20), which means we can evaluate $B(T_s)$ and $e^{-2\gamma T_s}$ at $T_s=T_3+T_{21}$ and integrate over T_s to obtain

$$S_{SE}=\frac{(k_sLnd)^2c}{128\epsilon_0}\left(\frac{\gamma_{3,2}}{\gamma_{3,1}+\gamma_{3,2}}\right)^2\frac{\sqrt{2\pi}}{ku}e^{-2\gamma_1 T_{32}}e^{-4\gamma T_{21}}\times B(T_s=T_3+T_{21}). \quad (22)$$

Each sine function in Eq. (21) is now expanded in a Taylor series,

$$\sin\Theta_j=\sum_{l=0}^{\infty}\frac{(-1)^l(\theta_j)^{2l+1}}{(2l+1)!}\exp\left\{-(2l+1)\left[\left(\frac{x-v_xT_{sj}}{x_j}\right)^2+\left(\frac{y-v_yT_{sj}}{y_j}\right)^2\right]\right\}. \quad (23)$$

Using $\int_{-\infty}^{+\infty}e^{-\alpha p^2+2\beta p}dp=\sqrt{\pi/\alpha}e^{(\beta^2/\alpha)}$, all the integrals in Eq. (21) can be performed analytically, term by term, in Cartesian coordinates. These integrations are done step by step in Appendix B to find $B(T_s)$ for the general SE case.

To present the essential physics, we specialize to the case of cylindrically symmetric transverse-field distributions with equal widths, $x_j=y_j=w$ for all j. Note that attempting to use the symmetry of the fields and the velocity distribution by transforming into cylindrical coordinates only complicates the basic, separable Gaussian integrals. We also take the most important experimental regime, where $(ku)^{-1}<T_{21}\ll\gamma^{-1}\ll T_{32}$, w/u, assuring that the atomic coherence does not degrade homogeneously between the first two pulses and following the final pulse. Setting $T_{21}\simeq 0$ and $T_s\simeq T_{32}=T$, after integration we have

$$B(T)=\sum_{l,m,n=0}^{\infty}\sum_{l',m',n'=0}^{\infty}(-1)^{l+l'+m+m'+n+n'}\frac{(\theta_1)^{2l+2l'+2}}{(2l+1)!(2l'+1)!}\frac{(\theta_2)^{2m+2m'+2}}{(2m+1)!(2m'+1)!}\frac{(\theta_3)^{2n+2n'+2}}{(2n+1)!(2n'+1)!}\times\left[1+(2l+2m+2)T^2\frac{u^2}{w^2}\right]^{-1}\left[1+(2l'+2m'+2)T^2\frac{u^2}{w^2}\right]^{-1}\times\pi w^2\left[2(l+l'+m+m'+n+n')+6-\frac{(2l+2m+2)^2T^2\frac{u^2}{w^2}}{1+(2l+2m+2)T^2\frac{u^2}{w^2}}-\frac{(2l'+2m'+2)^2T^2\frac{u^2}{w^2}}{1+(2l'+2m'+2)T^2\frac{u^2}{w^2}}\right]^{-1}. \quad (24)$$

For pulse areas of order unity, the sum converges rapidly. Each term in the sum can be identified as one term in the perturbative calculation of the echo energy to all orders in the three laser pulse amplitudes, including the effects of transverse motion. Each order is represented by a set of indices $\{l,m,n,l',m',n'\}$. However, the full sum is an exact result.

The transit effects are seen in the second and third lines of Eq. (24). The second line results from the integration over velocities in (21) and is related to the intensity of the echo field. The third line reflects the integration over transverse coordinates and is therefore a property of the radiated power of the echo field. Both lines are seen to depend on one dimensionless parameter, the effective transit rate through the Gaussian interaction region multiplied by the atomic travel time,

$$\tau\equiv\gamma_{tr}T=\frac{\sqrt{2}u}{w}T. \quad (25)$$

Clearly, the dependence of the echo energy is a complicated sum over products of Lorentzians for each order of perturbation theory, which cannot be accurately described by a single homogeneous decay rate. (In the limit that $\tau\ll 1$, transit-time effects are no longer important — the lingering transverse-field dependence is evident from the terms in the third line of Eq. (24) that remain. In other words, we have also treated the Gaussian intensity distribution to all orders, even if transit effects are negligible.)

For weak pulses ($\theta_j\ll 1$ for all j), Eq. (24) reduces to

$$B(T)=\theta_1^2\theta_2^2\theta_3^2\frac{\pi w^2}{2(1+\tau^2)(3+\tau^2)}, \quad (26)$$

the lowest-order perturbation result. For nonperturbative $\pi/2$ pulses ($\theta_1=\theta_2=\theta_3=\pi/2$), as are typical of most SE experiments, the sums in Eq. (24) that determine B converge by the fourth term in each index. In Fig. 2, we plot the echo signal $S_{SE}\propto B(T_s=T)$ versus τ with solid lines, for both [Fig. 2(a)] the weak pulse echo [Eq. (26)] and [Fig. 2(b)] the nonperturbative case [Eq. (24)]. The signals have been arbi-

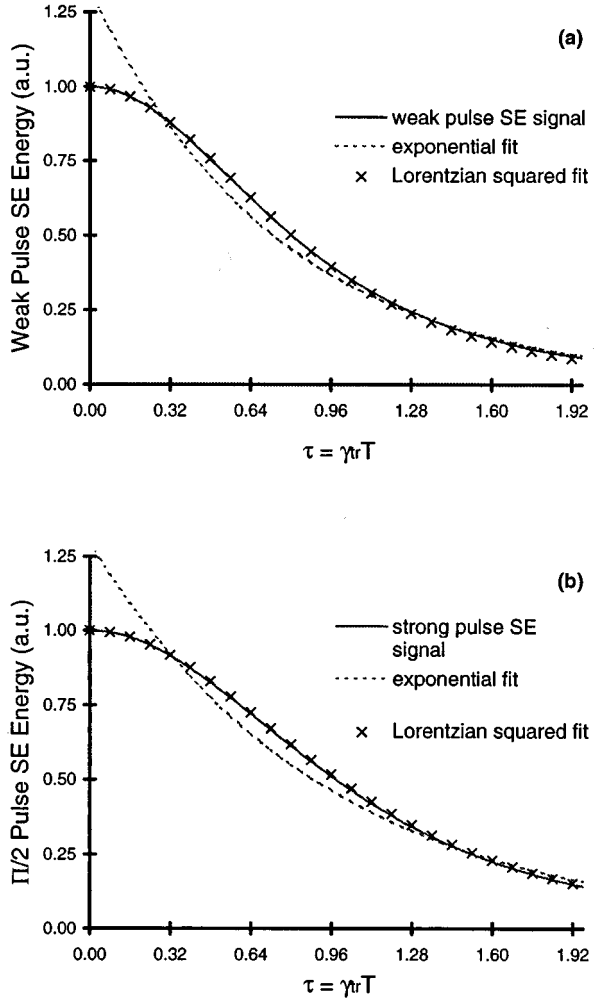

FIG. 2. (a) The weak-pulse SE signal of Eq. (26) is shown versus the dimensionless parameter τ, where $\tau=\gamma_{tr}T$ is defined by Eq. (25). (b) Strong ($\pi/2$)-pulse SE signal versus τ using Eq. (24). The exponential and Lorentzian-squared decay models are overlaid for comparison. The similarity of a Lorentzian-squared fit to the actual signal is evident from the weak-pulse SE expression, Eq. (26). These models, as discussed in the text, do not scale correctly with input pulse intensity. The exact SE signal, Eq. (24), does.

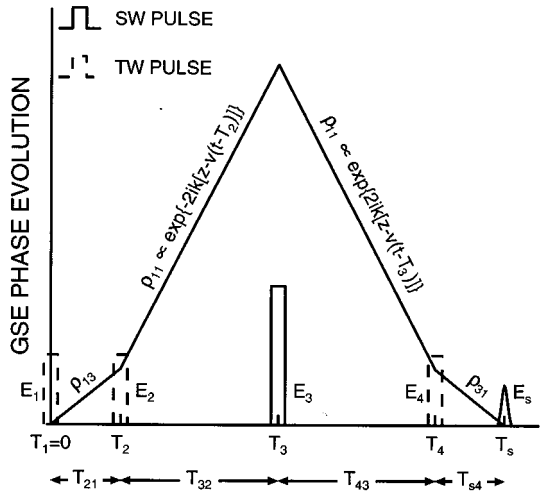

FIG. 3. Doppler phase diagram for the grating stimulated-photon echo (GSE). The phase of the density-matrix elements that contribute to a GSE signal is shown. The ground-state population ρ_{11} evolves with a Doppler phase for a time T_{42}. Rephasing is initiated by the standing wave pulse at T_3. The GSE signal at T_s travels in the $+\hat{\boldsymbol{z}}$ direction for a final TW laser pulse at T_4 in the $-\hat{\boldsymbol{z}}$ direction. Transit effects are significant for $T_{42}\gtrsim\gamma_{tr}^{-1}$, where γ_{tr} is defined by Eq. (25).

trarily scaled to match at $\tau=0$. For the weak-field case, the half width at half maximum (HWHM) of B in terms of τ can be found analytically from Eq. (26), $\Delta\tau_p=(7^{1/2}-2)^{1/2}=0.804$. From the computer-generated signal for $\pi/2$ pulse excitation, the HWHM is $\Delta\tau_{np}\cong 0.978$. The radiated energy for the nonperturbative case is seen to decay more slowly as T increases than for weak-field excitation. The ''x'' points in Fig. 2 indicate Lorentzian-squared fits $(1+a^2\tau^2)^{-2}$ using the HWHMs above, showing that a nearly indistinguishable but analytically incorrect fit can be made for both weak and $\pi/2$ pulses. For such a Lorentzian-squared ansatz, the constant, $a^2=(2^{1/2}-1)/(\Delta\tau)^2$, determines what might be assumed to be the effective transit rate, $\Gamma_{tr}=a\gamma_{tr}$. For the weak-pulse echo, $a\cong 0.801$, while for the strong pulse case, $a=0.658$, leading to the conclusion that the transit rate is intensity dependent. However, there are no free parameters in Eqs. (24) and (26). For a particular gas of mass M, given accurate measurements of w and the temperature, the transit rate γ_{tr} is fixed: we can compare our results directly with experimental data, removing the scaling ambiguity with respect to input pulse intensities that Thomas and Forber encountered [13,15].

To compare our calculation to another phenomenological decay model, an exponential fit to our signals using linear regression is shown in Fig. 2 with dashed lines for both the strong- and weak-pulse SE. This corresponds to adjusting γ_1 in Eq. (22) and setting $B(T_s)=1$ and $\gamma=0$. Assuming the SE signal is proportional to $e^{-2\Gamma_{tr}T}$ and using the $1/e$ times $\tau_{1/e}^{-1}$ of the weak- and strong-pulse fits, respectively, yield two different results for the effective transit rate $\Gamma_{tr}=\frac{1}{2}\gamma_{tr}\tau_{1/e}^{-1}$: (a) $\Gamma_{tr}\cong 0.96\gamma_{tr}$ and (b) $\Gamma_{tr}\cong 0.81\gamma_{tr}$. As a result, such a model would again lead to the erroneous measurement of a field-dependent transit rate, inconsistent with the fixed definition $\gamma_{tr}=(\sqrt{2}u)/w$ that enters into our results.

B. The grating stimulated-echo signal

A GSE Doppler phase diagram is shown in Fig. 3. The four-pulse sequence consists of two counterpropagating TW pulses, $k_1=-k_2=k$, followed by a SW pulse, and ending with another TW pulse, $k_4=-k$ [5]. All pulses have the same transverse-field distribution with $1/e$ point w. The first pulse again creates an atomic coherence $\tilde{\rho}_{13}$, and the second pulse modulates the ground-state population, producing an $e^{i(k_2-k_1)z}$ Fourier component. The time between these pulses is short, $T_{21}\ll(ku)^{-1},\gamma^{-1}$, to prevent dephasing. However, because pulses 1 and 2 counterpropagate, $k_2-k_1=-2k$, in contrast to the SE scheme where $k_2-k_1=0$. As a result, Doppler dephasing occurs in the populations during the time interval $T_{32}\gg(2ku)^{-1}$. The SW pulse at T_3 then scatters population from the e^{-i2kz} Fourier component into the e^{i2kz} component, reversing the Doppler dephasing in ρ_{11} for $T_{43}=T_{32}$. Since we see from Eq. (8a) that

$\rho_{11}(T_3^+)\sim\rho_{11}(T_3^-)\cos(\Theta_3\cos kz)$ and $\cos(\Theta_3\cos kz)=\sum_{n=-\infty}^{+\infty}J_{2n}(\Theta_3)e^{i2nkz}$, only the $n=2$ term can scatter the e^{-i2kz} Fourier component into the e^{i2kz} component. The TW pulse at T_4 couples this ground-state population to the atomic dipoles $\tilde{\rho}_{31}$, which radiate coherently at $T_s\simeq 2T_{21}+2T_{32}$. Momentum conservation requires that $k_s=k$.

Because of the above considerations, we set $T_{21}\simeq 0$ and $T_s\simeq T_4=2T_{32}=2T$. The time intervals $T_{32}=T_{43}=T$ are long. This fact is more significant for the GSE, since the phase of the ground-state population between the second and fourth pulses is velocity dependent, implying a greater sensitivity to velocity-changing collisions. This has been discussed at length in Refs. [5–7]. As developed above, our formalism ignores the dephasing effects of velocity-changing collisions on the diagonal density-matrix elements. This omission is discussed below in the Conclusion, Sec. IV.

The optical Bloch equations are solved for this scheme to find the coherence at T_s,

$$\tilde{\rho}_{31}(T_s,x,y,z,\mathbf{v})=-\frac{i}{16}W_0(\mathbf{v})\left(\frac{\gamma_{3,2}}{\gamma_{3,1}+\gamma_{3,2}}\right)^2 e^{-\gamma_1(T_{32}+T_{43})}\times e^{-ikv_z(T_s-T_4-2T_{32}+2T_{43}-T_{21})}\times\sin\Theta_1\sin\Theta_2 J_4(\Theta_3)\sin\Theta_4 e^{ikz}. \quad (27)$$

We see that the Doppler dephasing of the modulated population is exactly cancelled by the explicit choice of $T_{32}=T_{43}$. Substituting Eq. (27) into Eq. (18) and integrating over v_z and T_s, we find

$$S_{GSE}=\frac{(k_sLnd)^2c}{512\epsilon_0}\left(\frac{\gamma_{3,2}}{\gamma_{3,1}+\gamma_{3,2}}\right)^4\frac{\sqrt{2\pi}}{ku}e^{-4\gamma_1 T}B(T_s=2T). \quad (28)$$

The echo pulse, which is peaked at the time $T_s=T_4+T_{21}\approx T_4$, is separable from the excitation pulse at T_4 since the two counterpropagate with respect to one another. Again, we have carried along a homogeneous ground-state decay rate γ_1 for comparison to our results for which $\gamma_1\to 0$.

The calculation of $B(T_s)$ is nearly identical to the SE case. In fact, the power-series expansion of the Bessel function,

$$J_4(\Theta_3)=\sum_{p=0}^{\infty}(-1)^p\frac{\left(\frac{\theta_3}{2}\right)^{2p+4}}{p!(p+4)!}(H_3)^{2p+4}, \quad (29)$$

where the Gaussian H_j was defined in Eq. (9), allows us to adapt the SE result [Eq. (24)]: we replace $T\to 2T$ for the coefficients of l,l',m,m' and add in the terms $(2p+4)$ and $(2p'+4)$ in the appropriate places. The result for $B(T_s=2T)$ is

$$B(2T)=\pi w^2\sum_{l,m,n,p=0}^{\infty}\sum_{l',m',n',p'=0}^{\infty}(-1)^{l+l'+m+m'+n+n'+p+p'}\times\frac{(\theta_1)^{2l+2l'+2}}{(2l+1)!(2l'+1)!}\frac{(\theta_2)^{2m+2m'+2}}{(2m+1)!(2m'+1)!}\frac{\left(\frac{\theta_3}{2}\right)^{2p+2p'+8}}{p!(p+4)!p'!(p'+4)!}\frac{(\theta_4)^{2n+2n'+2}}{(2n+1)!(2n'+1)!}\times\left[1+[4(2l+2m+2)+2p+4]\frac{T^2u^2}{w^2}\right]^{-1}\left[1+[4(2l'+2m'+2)+2p'+4]\frac{T^2u^2}{w^2}\right]^{-1}\times\left[2(l+l'+m+m'+n+n'+p+p')+14-\frac{[2(2l+2m+2)+2p+4]^2\frac{T^2u^2}{w^2}}{1+[4(2l+2m+2)+2p+4]\frac{T^2u^2}{w^2}}-\frac{[2(2l'+2m'+2)+2p'+4]^2\frac{T^2u^2}{w^2}}{1+[4(2l'+2m'+2)+2p'+4]\frac{T^2u^2}{w^2}}\right]^{-1}. \quad (30)$$

The structure of $B(T_s)$ for the GSE signal is similar to that of the SE. In lowest-order perturbation theory, the result is

$$B(2T)=\theta_1^2\theta_2^2\theta_4^2\left(\frac{\theta_3}{2}\right)^8\left(\frac{1}{4!}\right)^2\frac{\pi w^2}{2(1+6\tau^2)(7+10\tau^2)}. \quad (31)$$

We use the same definition of τ (25) for consistency, although the time scale of a GSE experiment $(2T)$ need not be the same as the time scale for a SE experiment (T). In Figs. 4(a) and 4(b), we plot $B(T_s=2T)$ versus τ for the weak-pulse GSE [Eq. (31)] and the nonperturbative GSE [Eq. (30)], respectively. For the nonperturbative case [Fig. 4(b)], we take the peak pulse areas $\theta_1=\theta_2=\theta_4=\pi/2$, as before,

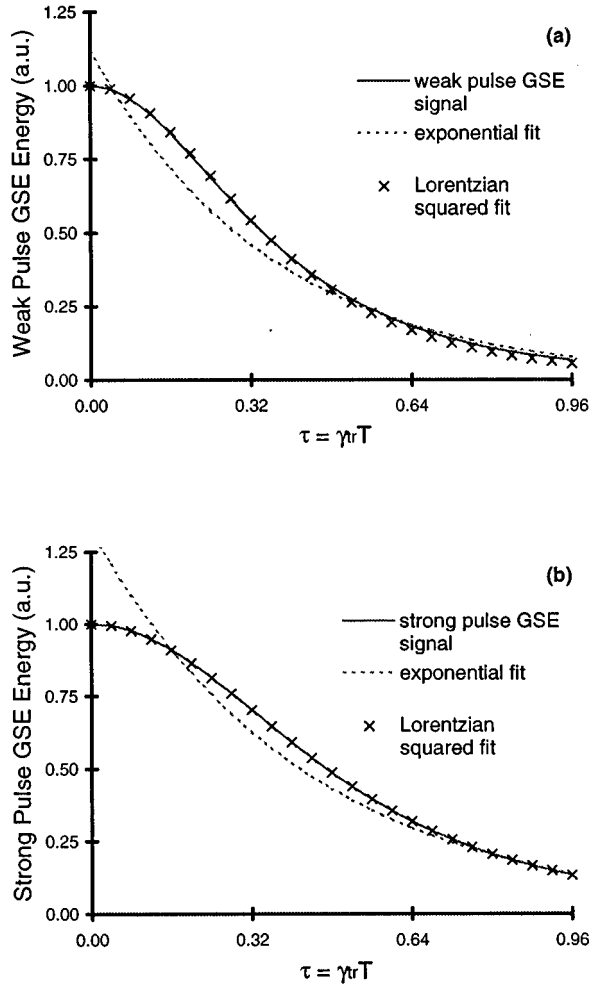

FIG. 4. (a) Weak-pulse GSE signal of Eq. (31) versus τ. (b) Strong-pulse GSE signal of Eq. (30) versus τ. Again, exponential and Lorentzian-squared fits are shown for comparison.

and we set θ_3 to maximize $J_4(\theta_3)$. This maximum occurs at $J_4(\theta_3 \approx 5.3) \simeq 0.4$. The similarity of the SE [Eq. (26)] and GSE [Eq. (31)] perturbation results is self-evident. For the calculated nonperturbative case, the measured HWHM is $\Delta\tau_{np} = 0.469$, compared to the analytical, perturbative result from Eq. (31), $\Delta\tau_p = [(274^{1/2} - 13)/30]^{1/2} = 0.344$. For completeness, in Fig. 4, an exponential fit to each signal is superimposed with dashed lines, and the excellent Lorentzian-squared fits are marked by ''x.'' The asymptotic deviation of the Lorentzian fit to the perturbation result is evident in Fig. 4(a).

Taking into account the time scale of the GSE experiment $2T$, we again conclude that these fits lead to inconsistent transit times for different excitation pulse strengths. For the exponential fit, assuming from Eq. (28) that the GSE signal is proportional to $e^{-4\Gamma_{tr}T}$, the effective transit rates $\Gamma_{tr} = \frac{1}{4}\gamma_{tr}\tau_{1/e}^{-1}$ for the weak- and strong-pulse cases are (a) $\Gamma_{tr} \cong 0.70\gamma_{tr}$ and (b) $\Gamma_{tr} \cong 0.59\gamma_{tr}$, respectively. Using $(1+a^2\tau^2)^{-2}$ for the Lorentzian-squared fits, the effective transit rates $\Gamma_{tr} = (a/2)\gamma_{tr}$ are (a) $\Gamma_{tr} = 0.935\gamma_{tr}$ and (b) $\Gamma_{tr} \cong 0.686\gamma_{tr}$, respectively. Despite the excellent fit of the Lorentzian-squared decay functions for both the SE and GSE signals, we have shown that the essential physics makes sense only in the context of the sum over the product of Lorentzian functions shown in Eqs. (24) and (30), which are accurate for arbitrary input pulse areas.

IV. CONCLUSION

In this paper, we have demonstrated a method for including transit-time effects in coherent transient calculations for short laser pulses with Gaussian spatial profiles interacting with atomic vapors. Using this method, we have derived nonperturbative expressions for the SE and GSE signals as a function of the relevant pulse delays. By comparing these signals to phenomenological decay models in both the strong (nonperturbative) and weak (perturbative) excitation pulse cases, we have shown the necessity of our analysis in interpreting an experimental measurement of the transit rate. Strong pulse echoes are seen to decay more slowly as a function of time delay than weak pulse echoes. And in either case, the bell-shaped decay as a function of the dimensionless parameter τ are poorly fit by any exponential loss rate. To our knowledge, this paper is the first rigorous derivation of Gaussian-beam transit effects in photon echo spectroscopy.

Our analysis has relied on an assumption of classical, ballistic transport for the atoms. When atom-perturber collisions are considered, the master equations become more complicated, especially for the diagonal density matrix elements [6,16]. If we assume the off-diagonal elements decay homogeneously with the collision rate Γ, as in Eq. (5c), we must still alter Eqs. (5a) and (5b) for the diagonal elements by adding the terms

$$\left[\frac{d}{dt}\rho_{aa}(\mathbf{v},\mathbf{R},t)\right]_{coll} = -\Gamma_a(\mathbf{v})\rho_a(\mathbf{v},\mathbf{R},t) + \int d\mathbf{v}'\, W_a(\mathbf{v}' \rightarrow \mathbf{v})\rho_{aa}(\mathbf{v}',\mathbf{R},t) \tag{32}$$

for $a = \{1,3\}$. This expression will affect only the field-free regions, so Eqs. (11a)–(11d) are no longer valid. The first term in Eq. (32) represents the total collisional decay of atoms out of the state a population with velocity $\mathbf{v}$ with rate $\Gamma_a(\mathbf{v}) = \int d\mathbf{v}' W_a(\mathbf{v} \rightarrow \mathbf{v}')$, while the second is the term for scattering into level a with velocity $\mathbf{v}$. The collision kernel $W_a(\mathbf{v}' \rightarrow \mathbf{v})$, defined as the transition probability density per unit time for the atom to scatter from velocity $\mathbf{v}'$ to $\mathbf{v}$, can be calculated quantum mechanically from the atom-perturber scattering amplitude and is complex enough to make the kind of analytical solutions we have derived for photon echo signals nearly impossible.

In general, for a vapor in thermal equilibrium, detailed balance requires that the kernel lead toward a Maxwellian velocity distribution for the density matrix in the long-time limit; as a result, $W_a(\mathbf{v}' \rightarrow \mathbf{v}) \neq W_a(\mathbf{v} - \mathbf{v}')$ and physical collision kernels do not have nice Fourier transform-convolution properties in velocity space. This has been discussed at length for spatially homogeneous systems in Refs. [6,16]. For our calculations, where the density matrix depends strongly on the transverse coordinate, the propagator of the diagonal density matrix valid for the field-free regions

must be a separable exponential or Gaussian function of the coordinates and velocities to be treated easily in our model, independent of the kernel that determines its exact analytic form. Such is the case for the Gaussian propagator of the Fokker-Planck transport equation in coordinate-velocity phase space [17], relevant for Brownian motion in the weak-collision regime [6]. So, for this limiting case of atomic diffusion, we can again derive analytical results. It is the transition regime from ballistic to diffusive transport that makes analytic calculations difficult. And for any inclusion of velocity-changing collisions, the mathematics of propagating the density matrix between laser pulses is more complicated and will not be considered here.

However, we can make some general remarks about transit effects in probing collision processes using the above echo techniques. For the SE, any collisions that cause a change in velocity between pulses 2 and 3 make it difficult to rephase the atoms and tend to destroy the echo signal. Despite this, use of a diffusion model of atomic motion allows for explicit calculations of the SE intensity as a function of time. Physically, the first and second laser pulses pick out a cylinder of atoms that can contribute to the echo. This cylinder then diffuses outward until the final pulse arrives. But, if the time interval T_{32} is long enough to be in the diffusive regime of atomic motion, the velocity of the atom at T_3 is uncorrelated with its velocity at T_2 and cancellation of the Doppler phase built up in the time T_{21} becomes impossible.

For the GSE, collisions have been considered in depth previously [6]. They can be used to probe collision processes for the velocity-sensitive populations between pulses 2 and 4. A revival of the GSE signal in the high-pressure regime, where the mean free path of each atom is less than a wavelength, has been predicted and is related to collective atomic coherence effects and Dicke narrowing. In this case, no Doppler phase for the populations can build up in the T_{32} and T_{43} time intervals: the atoms that can contribute to the echo signal have a time-averaged velocity of zero and tend to be trapped in the laser beam cylinder. This can be understood schematically by noting that

$$\bar{\mathbf{v}} \propto \int_{T_2}^{T_3} \mathbf{v}(t)\,dt = 0 \Rightarrow \exp\left[i2k \int_{T_2}^{T_3} v_z(t)\,dt \right] = 1. \tag{33}$$

It would be interesting to correlate the GSE signal in different pressure regimes with the transition from ballistic to diffusive atomic motion. As for the SE, GSE theoretical echo expressions, including center-of-mass motion, can be calculated using the propagator of the Fokker-Planck equation with an experimentally determined diffusion constant in the high-pressure regime.

ACKNOWLEDGMENTS

The authors would like to thank B. Dubetsky and J. E. Thomas for their time and effort adding insight to this work. J.L.C. would also like to thank Professor Max Cohen for his steadfast support. This work was supported by the National Science Foundation through Grant No. PHY-94114020 and by the U. S. Army Research Office under Grant No. DAAHO4-93-G-0503.

APPENDIX A: GENERALIZED ECHO SIGNALS

The form of the atomic coherence from Eqs. (8a)–(8d) (9), and (11a)–(11d) is always

$$\begin{aligned}\tilde{\rho}_{31}(t=T_s,x,y,z,\mathbf{v}) &= -i\left(\frac{1}{2}\right)^N W_1(\mathbf{v}) F(T_1,\ldots,T_N,T_s,k_1,\ldots,k_N,z,v_z) \\ &\quad \times \prod_{j=1}^{N} G_j(\Theta_j).\end{aligned} \tag{A1}$$

The function F is a product of rates and exponential factors containing the temporal decay and phase, as well as the z-dependent spatial phase, of $\tilde{\rho}_{31}$. From Eqs. (8a)–(8d) each function G_j in (A1) must be one of the following:

$$G_j = \begin{cases} \sin\Theta_j \\ 1 \pm \cos\Theta_j, \\ J_q(\Theta_j) \end{cases} \tag{A2}$$

where J_q is the qth order Bessel function of the first kind. The integer q is determined by the phase-matching condition on k_s: given that $k_s = \pm k$, typically only a single q can contribute to the echo signal.

Using the definition of the echo signal in Eq. (18) and inserting (A1),

$$\begin{aligned} S = \left(\frac{1}{2}\right)^{2N+1} \frac{(kLnd)^2 c}{\epsilon_0} \int dT_s \Bigg[\int\int dx\,dy \\ \times \left| \int\int \frac{dv_x dv_y}{(\pi u^2)} e^{-(v_x^2+v_y^2)/u^2} \prod_j G_j(\Theta_j) \right|^2 \Bigg] \\ \times \left| \int \frac{dv_z}{(\pi u^2)^{1/2}} F e^{-ik_s z} e^{-v_z^2/u^2} \right|^2. \end{aligned} \tag{A3}$$

Since F is independent of x, y, v_x, and v_y, the integral over the longitudinal velocity v_z has been separated from the integrals over the transverse coordinates and velocities and appears at the end of Eq. (A3). This integral determines the Doppler rephasing time that maximizes the echo and in general can be shown to give

$$\begin{aligned} &\left| \int \frac{dv_z}{(\pi u^2)^{1/2}} F e^{-ik_s z} e^{-v_z^2/u^2} \right|^2 \\ &\quad = \exp\left[-\frac{(ku)^2}{2} [T_s - (T_N + \Delta T)]^2 \right] \\ &\quad \times (\text{decay terms}), \end{aligned} \tag{A4}$$

where the Gaussian temporal envelope of the echo intensity is centered at a time ΔT after the final excitation pulse at T_N. The unspecified ''decay terms'' in Eqs. (A4) depend on the specific echo scheme and are the homogeneous terms derived from Eqs. (11a)–(11d). In the Doppler limit they always vary slowly compared to the Gaussian temporal envelope. The discussion following Eqs. (11a)–(11d) suggests that their time dependence can often be neglected for long echo experiments involving the modulated ground state.

The main result of this paper, which is the determination of transit-time effects, is represented by the square bracket of Eq. (A3),

$$B(T_1,\ldots,T_N,T_s) = \left[\int\int dxdy\left|\int\int \frac{dv_x dv_y}{(\pi u^2)} e^{-(v_x^2+v_y^2)/u^2}\prod_j G_j(\Theta_j)\right|^2\right]. \tag{A5}$$

From Eq. (A3), we see that $B(T_1,\ldots,T_N,T_s)$ is essentially the peak power of the echo field [18]. Given the Gaussian transverse distributions H_j, we expand each $G_j(\Theta_j)$ in a Taylor series; for example,

$$1-\cos\Theta_j = 2\sin^2\frac{\Theta_j}{2} = 2\sum_{m,n=0}^{\infty}\frac{(-1)^{m+n}(\theta_j/2)^{2m+2n+2}}{(2m+1)!(2n+1)!}H_j^{2m+2n+2}. \tag{A6}$$

All of the integrals in Eq. (A5) can now be performed analytically, term by term. Substituting Eqs. (A4) and (A5) into Eq. (A3),

$$S=\left(\frac{1}{2}\right)^{2N+1}\frac{(kLnd)^2 c}{\epsilon_0}\int dT_s B(T_1,\ldots,T_N,T_s) \times\exp\left[-\frac{(ku)^2}{2}[T_s-(T_N+\Delta T)]^2\right]\times(\text{decay terms}). \tag{A7}$$

In the transit regime of interest, where $ku\gg\gamma_{tr}$, $B(T_1,\ldots,T_N,T_s)$ varies slowly in time compared to the Gaussian temporal envelope. We therefore pull the slowly varying functions out of the integrand, evaluating them at the peak of the Gaussian $T_s=T_N+\Delta T$, and integrate over the Gaussian. This yields our final result for the echo signal,

$$S=\left(\frac{1}{2}\right)^{2N+1}\frac{(kLnd)^2 c}{\epsilon_0}\frac{\sqrt{2\pi}}{ku}B(T_1,\ldots,T_N,T_s=T_N+\Delta T) \times(\text{decay terms})_{T_s=T_N+\Delta T}. \tag{A8}$$

The echo energy is only a function of the times between pulses. This is a known, general result. To derive more physical intuition for transit effects, Sec. III examines the exact form of $B(T_1,\ldots,T_N,T_s)$ for the SE [Eq. (24)] and the GSE [Eq. (30)], respectively.

APPENDIX B: TRANSVERSE INTEGRALS FOR THE SE CALCULATION

The integration of Eq. (21) is straightforward, using the power series expansion of $\sin\Theta_j$ (23):

$$\begin{aligned}B(T_s) &= \int\int dx\,dy\left|\int\int\frac{dv_x dv_y}{\pi u^2}e^{-(v_x^2+v_y^2)/u^2} \times\sin\Theta_1\sin\Theta_2\sin\Theta_3\right|^2 \\ &= \int\int dx\,dy\left|\sum_{l,m,n=0}^{\infty}(-1)^{l+m+n}\frac{(\theta_1)^{2l+1}}{(2l+1)!} \times\frac{(\theta_2)^{2m+1}}{(2m+1)!}\frac{(\theta_3)^{2n+1}}{(2n+1)!}\int\int\frac{dv_x dv_y}{\pi u^2} \times e^{-(v_x^2+v_y^2)/u^2}H_1^{2l+1}H_2^{2m+1}H_3^{2n+1}\right|^2,\end{aligned} \tag{B1}$$

where H_j is given in Eq. (9). Separating the v_x and v_y integrals, the v_x integration proceeds as

$$\begin{aligned}&\int\frac{dv_x}{\sqrt{\pi u^2}}e^{-v_x^2/u^2}\exp\left[-(2l+1)\left(\frac{x-v_x T_{s1}}{x_1}\right)^2\right] \times\exp\left[-(2m+1)\left(\frac{x-v_x T_{s2}}{x_2}\right)^2\right] \times\exp\left[-(2n+1)\left(\frac{x-v_x T_{s3}}{x_3}\right)^2\right] \\ &=\exp\left[-x^2\left(\frac{2l+1}{x_1^2}+\frac{2m+1}{x_2^2}+\frac{2n+1}{x_3^2}\right)\right]\int\frac{dv_x}{\sqrt{\pi u^2}} \times\exp\left[-v_x^2\left(\frac{1}{u^2}+\frac{(2l+1)T_{s1}^2}{x_1^2}+\frac{(2m+1)T_{s2}^2}{x_2^2} +\frac{(2n+1)T_{s3}^2}{x_3^2}\right)\right]\exp\left[+2v_x x\left(\frac{(2l+1)T_{s1}}{x_1^2} +\frac{(2m+1)T_{s2}}{x_2^2}+\frac{(2n+1)T_{s3}}{x_3^2}\right)\right].\end{aligned} \tag{B2}$$

Now, we use $\int_{-\infty}^{+\infty}e^{-\alpha p^2}e^{2\beta p}dp=\sqrt{\pi/\alpha}\;e^{(\beta^2/\alpha)}$, to give

$$\int \frac{dv_x}{\sqrt{\pi u^2}}\cdots=\exp\left[-x^2\left(\frac{2l+1}{x_1^2}+\frac{2m+1}{x_2^2}+\frac{2n+1}{x_3^2}\right)\right]\exp\left[x^2\frac{\left(\frac{(2l+1)T_{s1}}{x_1^2}+\frac{(2m+1)T_{s2}}{x_2^2}+\frac{(2n+1)T_{s3}}{x_3^2}\right)^2}{\left(\frac{1}{u^2}+\frac{(2l+1)T_{s1}^2}{x_1^2}+\frac{(2m+1)T_{s2}^2}{x_2^2}+\frac{(2n+1)T_{s3}^2}{x_3^2}\right)}\right]$$
$$\times\left[1+\frac{(2l+1)T_{s1}^2u^2}{x_1^2}+\frac{(2m+1)T_{s2}^2u^2}{x_2^2}+\frac{(2n+1)T_{s3}^2u^2}{x_3^2}\right]^{-1/2}. \tag{B3}$$

The integration over v_y also gives Eq. (B3) with the replacements $x\rightarrow y$ and $x_j\rightarrow y_j$.

Putting these expressions into Eq. (B1) and squaring the sums using $(\Sigma_l f_l)^2=\Sigma_l\Sigma_{l'}f_lf_{l'}$, we still have to perform the integrations over x and y,

$$\int\int dx\,dy\cdots=\int dx\exp\left[-x^2\left(\frac{2l+2l'+2}{x_1^2}+\frac{2m+2m'+2}{x_2^2}+\frac{2n+2n'+2}{x_3^2}\right)\right]$$
$$\times\exp\left[x^2\left(\frac{\left(\frac{(2l+1)T_{s1}}{x_1^2}+\frac{(2m+1)T_{s2}}{x_2^2}+\frac{(2n+1)T_{s3}}{x_3^2}\right)^2}{\frac{1}{u^2}+\frac{(2l+1)T_{s1}^2}{x_1^2}+\frac{(2m+1)T_{s2}^2}{x_2^2}+\frac{(2n+1)T_{s3}^2}{x_3^2}}\right.\right.$$
$$\left.\left.+\frac{\left(\frac{(2l'+1)T_{s1}}{x_1^2}+\frac{(2m'+1)T_{s2}}{x_2^2}+\frac{(2n'+1)T_{s3}}{x_3^2}\right)^2}{\frac{1}{u^2}+\frac{(2l'+1)T_{s1}^2}{x_1^2}+\frac{(2m'+1)T_{s2}^2}{x_2^2}+\frac{(2n'+1)T_{s3}^2}{x_3^2}}\right)\right]$$
$$\times\int dy\exp\left[-y^2\left(\frac{2l+2l'+2}{y_1^2}+\frac{2m+2m'+2}{y_2^2}+\frac{2n+2n'+2}{y_3^2}\right)\right]$$
$$\times\exp\left[y^2\left(\frac{\left(\frac{(2l+1)T_{s1}}{y_1^2}+\frac{(2m+1)T_{s2}}{y_2^2}+\frac{(2n+1)T_{s3}}{y_3^2}\right)^2}{\frac{1}{u^2}+\frac{(2l+1)T_{s1}^2}{y_1^2}+\frac{(2m+1)T_{s2}^2}{y_2^2}+\frac{(2n+1)T_{s3}^2}{y_3^2}}\right.\right.$$
$$\left.\left.+\frac{\left(\frac{(2l'+1)T_{s1}}{y_1^2}+\frac{(2m'+1)T_{s2}}{y_2^2}+\frac{(2n'+1)T_{s3}}{y_3^2}\right)^2}{\frac{1}{u^2}+\frac{(2l'+1)T_{s1}^2}{y_1^2}+\frac{(2m'+1)T_{s2}^2}{y_2^2}+\frac{(2n'+1)T_{s3}^2}{y_3^2}}\right)\right]. \tag{B4}$$

Again, the integrations over x and y separate. The x integration gives

$$\frac{\sqrt{\pi}}{\left[\frac{2l+2l'+2}{x_1^2}+\frac{2m+2m'+2}{x_2^2}+\frac{2n+2n'+2}{x_3^2}-\frac{\left(\frac{(2l+1)T_{s1}}{x_1^2}+\frac{(2m+1)T_{s2}}{x_2^2}+\frac{(2n+1)T_{s3}}{x_3^2}\right)^2}{\frac{1}{u^2}+\frac{(2l+1)T_{s1}^2}{x_1^2}+\frac{(2m+1)T_{s2}^2}{x_2^2}+\frac{(2n+1)T_{s3}^2}{x_3^2}}-\frac{\left(\frac{(2l'+1)T_{s1}}{x_1^2}+\frac{(2m'+1)T_{s2}}{x_2^2}+\frac{(2n'+1)T_{s3}}{x_3^2}\right)^2}{\frac{1}{u^2}+\frac{(2l'+1)T_{s1}^2}{x_1^2}+\frac{(2m'+1)T_{s2}^2}{x_2^2}+\frac{(2n'+1)T_{s3}^2}{x_3^2}}\right]^{1/2}}, \tag{B5}$$

and the y integration is found by replacing $x_j\rightarrow y_j$. The final result for $B(T_s)$ shows the effect of transverse motion on the SE signal,

$$B=\sum_{l,m,n=0}^{\infty}\sum_{l',m',n'=0}^{\infty}(-1)^{l+l'+m+m'+n+n'}\frac{(\theta_1)^{2l+2l'+2}}{(2l+1)!(2l'+1)!}\frac{(\theta_2)^{2m+2m'+2}}{(2m+1)!(2m'+1)!}\frac{(\theta_3)^{2n+2n'+2}}{(2n+1)!(2n'+1)!}$$

$$\times\left[1+\left(\frac{(2l+1)T_{s1}^2}{x_1^2}+\frac{(2m+1)T_{s2}^2}{x_2^2}+\frac{(2n+1)T_{s3}^2}{x_3^2}\right)u^2\right]^{-1/2}\left[1+\left(\frac{(2l'+1)T_{s1}^2}{x_1^2}+\frac{(2m'+1)T_{s2}^2}{x_2^2}+\frac{(2n'+1)T_{s3}^2}{x_3^2}\right)u^2\right]^{-1/2}$$

$$\times\left[1+\left(\frac{(2l+1)T_{s1}^2}{y_1^2}+\frac{(2m+1)T_{s2}^2}{y_2^2}+\frac{(2n+1)T_{s3}^2}{y_3^2}\right)u^2\right]^{-1/2}\left[1+\left(\frac{(2l'+1)T_{s1}^2}{y_1^2}+\frac{(2m'+1)T_{s2}^2}{y_2^2}+\frac{(2n'+1)T_{s3}^2}{y_3^2}\right)u^2\right]^{-1/2}$$

$$\times\frac{\sqrt{\pi}}{\left[\dfrac{2l+2l'+2}{x_1^2}+\dfrac{2m+2m'+2}{x_2^2}+\dfrac{2n+2n'+2}{x_3^2}-\dfrac{\left(\dfrac{(2l+1)T_{s1}}{x_1^2}+\dfrac{(2m+1)T_{s2}}{x_2^2}+\dfrac{(2n+1)T_{s3}}{x_3^2}\right)^2}{\dfrac{1}{u^2}+\dfrac{(2l+1)T_{s1}^2}{x_1^2}+\dfrac{(2m+1)T_{s2}^2}{x_2^2}+\dfrac{(2n+1)T_{s3}^2}{x_3^2}}-\dfrac{\left(\dfrac{(2l'+1)T_{s1}}{x_1^2}+\dfrac{(2m'+1)T_{s2}}{x_2^2}+\dfrac{(2n'+1)T_{s3}}{x_3^2}\right)^2}{\dfrac{1}{u^2}+\dfrac{(2l'+1)T_{s1}^2}{x_1^2}+\dfrac{(2m'+1)T_{s2}^2}{x_2^2}+\dfrac{(2n'+1)T_{s3}^2}{x_3^2}}\right]^{1/2}}$$

$$\times\frac{\sqrt{\pi}}{\left[\dfrac{2l+2l'+2}{y_1^2}+\dfrac{2m+2m'+2}{y_2^2}+\dfrac{2n+2n'+2}{y_3^2}-\dfrac{\left(\dfrac{(2l+1)T_{s1}}{y_1^2}+\dfrac{(2m+1)T_{s2}}{y_2^2}+\dfrac{(2n+1)T_{s3}}{y_3^2}\right)^2}{\dfrac{1}{u^2}+\dfrac{(2l+1)T_{s1}^2}{y_1^2}+\dfrac{(2m+1)T_{s2}^2}{y_2^2}+\dfrac{(2n+1)T_{s3}^2}{y_3^2}}-\dfrac{\left(\dfrac{(2l'+1)T_{s1}}{y_1^2}+\dfrac{(2m'+1)T_{s2}}{y_2^2}+\dfrac{(2n'+1)T_{s3}}{y_3^2}\right)^2}{\dfrac{1}{u^2}+\dfrac{(2l'+1)T_{s1}^2}{y_1^2}+\dfrac{(2m'+1)T_{s2}^2}{y_2^2}+\dfrac{(2n'+1)T_{s3}^2}{y_3^2}}\right]^{1/2}}. \tag{B6}$$

Substitution of Eq. (B6) into (20) or (22) gives the echo energy for this general SE scheme. The quantity $B(T_s)$ simplifies to Eq. (24) for $x_j=y_j=w$, $T_{s3}=0$, and $T_{s1}=T_{s2}=T$.

[1] The following references contain detailed reviews of coherent transient spectroscopy: R.G. Brewer, in *Frontiers in Laser Spectroscopy*, edited by R. Balian, S. Haroche, and S. Liberman (North-Holland, Amsterdam, 1977); R.L. Shoemaker, in *Laser and Coherence Spectroscopy*, edited by J.I. Steinfeld (Plenum, New York, 1978); M.D. Levenson, and S.S. Kano, *Introduction to Nonlinear Laser Spectroscopy*, revised edition (Academic Press, New York, 1988), Chap. 6.

[2] For a review of echo processes in vapors up to 1979, see T.W. Mossberg, R.K. Kachru, S.R. Hartmann, and A.M. Flusberg, Phys. Rev. A **20**, 1976 (1979).

[3] Echoes in standing-wave light fields were first observed and explained in the following papers: V.P. Chebotayev, N.M. Dyuba, M.I. Skvortsov, and L.S. Vasilenko, Appl. Phys. **15**, 319 (1978); T.W. Mossberg, R.K. Kachru, E. Whittaker, and S.R. Hartmann, Phys. Rev. Lett. **43**, 851 (1979); R.K. Kachru, T.W. Mossberg, E. Whittaker, and S.R. Hartmann, Opt. Commun. **31**, 223 (1979); J.L. Le Gouët and P.R. Berman, Phys. Rev. A **20**, 1105 (1979).

[4] For photon echo spectroscopy where one of the laser pulses is long (i.e., pulse duration on the order of relaxation times), see A.G. Yodh, J. Golub, and T.W. Mossberg, Phys. Rev. Lett. **53**, 659 (1984); R. Sung and P.R. Berman, Phys. Rev. A **39**, 6284 (1989); R. Sung and P.R. Berman, Phys. Rev. A **39**, 6298 (1989).

[5] For novel echo effects introduced recently as grating stimulated echoes, see B. Dubetsky, P.R. Berman, and T. Sleator, Phys. Rev. A **46**, R2213 (1992).

[6] P.R. Berman, Phys. Rev. A **49**, 2922 (1994).

[7] B. Dubetsky and P.R. Berman, Laser Phys. **4**, 1017 (1994).

[8] N.A. Kurnit, I.D. Abella, and S.R. Hartmann, Phys. Rev. Lett **13**, 567 (1964).

[9] J.E. Bjorkholm, P.F. Liao, and A. Wokaun, Phys. Rev. A **26**, 2643 (1982); R.A. Forber, L. Spinelli, J.E. Thomas, and M.S. Feld, Phys. Rev. Lett. **50**, 331 (1983); E. Buhr and J. Mlynek, Phys. Rev. Lett. **57**, 1300 (1986); L.S.Vasilenko, N.N. Rubtsova, and E.B. Khvorostov, Pis'ma Zh. Eksp. Teor. Fiz. **62**, 393 (1995) [JETP Lett. **62**, 404 (1995)].

[10] The literature contains perturbative calculations of transit-time broadening in both Doppler-broadened and Doppler-free saturation spectroscopy: S.G. Rautian and A.M. Shalagin, Pis'ma Zh. Eksp. Teor. Fiz. **58**, 962 (1970) [Soviet Phys. JETP **31**, 518 (1970)]; J.E. Thomas, M.J. Kelly, J.P. Monchalin, N.A. Kurnit, and A. Javan, Phys. Rev. A **15**, 2356 (1977); V.A. Alekseev and L.P. Yatsenko, Pis'ma Zh. Eksp. Teor. Fiz. **77**, 2254 (1979) [Soviet JETP **50**, 1083 (1979)]; J.E. Thomas and W.W. Quivers, Phys. Rev. A **22**, 2115 (1980); B.Ya. Dubetskii and V.M. Semibalamut, Soviet J. Quantum Electron. **17**, 1495 (1987).

[11] W. Gawlik, Phys. Rev A **34**, 3760 (1986).

[12] For inclusion of the transverse-beam profile in the perturbative density-matrix formalism for Ramsey fringes, see C.J. Bordé, in *Advances in Laser Spectroscopy*, edited by F.T. Arecchi, F. Strumla, and H. Walther (Plenum, New York, 1983), and references therein.

[13] J.E. Thomas and R.A. Forber, Opt. Lett. **9**, 56 (1984).

[14] P. Meystre and M. Sargent III, *Elements of Quantum Optics*, 2nd ed. (Springer-Verlag, Berlin, 1991) addresses photon echoes in both an amplitude and Bloch vector formalism. Neither are adequate to describe the decay scheme of the atom in Fig. 1.

[15] For the basic, two-pulse echo experiment, as outlined in the Introduction above, $B(T_s=2T)$ can be adapted with experience from (24). Using (23) and (A6),

$$B(2T)=\int\int dx\,dy\left|\int\int\frac{dv_x dv_y}{\pi u^2}e^{-(v_x^2+v_y^2)/u^2}\sin\Theta_1(1-\cos\Theta_2)\right|^2$$

$$=2\pi w^2\sum_{l,m,n=0}^{\infty}\sum_{l',m',n'=0}^{\infty}(-1)^{l+l'+m+m'+n+n'}\frac{(\theta_1)^{2l+2l'+2}}{(2l+1)!(2l'+1)!}\frac{\left(\frac{\theta_2}{2}\right)^{2m+2n+2m'+2n'+4}}{(2m+1)!(2n+1)!(2m'+1)!(2n'+1)!}$$

$$\times\left[1+[4(2l+1)+2m+2n+2]T^2\frac{u^2}{w^2}\right]^{-1}\left[1+[4(2l'+1)+2m'+2n'+2]T^2\frac{u^2}{w^2}\right]^{-1}$$

$$\times\frac{1}{2(l+l'+m+m'+n+n')+6-\dfrac{[2(2l+1)+2m+2n+2]^2T^2\dfrac{u^2}{w^2}}{1+[4(2l+1)+2m+2n+2]T^2\dfrac{u^2}{w^2}}-\dfrac{[2(2l'+1)+2m'+2n'+2]^2T^2\dfrac{u^2}{w^2}}{1+[4(2l'+1)+2m'+2n'+2]T^2\dfrac{u^2}{w^2}}}.$$

From this expression the lowest-order perturbation result for the basic photon echo signal is

$$S(2T)\sim e^{-4\gamma T}\frac{\pi w^2\theta_1^2\left(\frac{\theta_2}{2}\right)^4}{(1+3\tau^2)(3+\tau^2)}.$$

This signal is seen to differ from the perturbative expression derived by Thomas and Forber in Ref. [13]. These results should allow for a theoretical fit to their data without free parameters, where their τ_{tr} and γ_s are our γ_{tr}^{-1} and 2γ, respectively. From (25), for a laser beam 1/e intensity diameter $\sqrt{2}w=1$ mm and $u=2.5\times10^5$mm/s, $\tau_{tr}=\gamma_{tr}^{-1}=w/\sqrt{2}u=2$ μs. This corresponds to a typical rubidium experiment at room temperature. Finally, $\tau=T/\tau_{tr}$, and their signal for weak pulse excitation may be expressed as

$$\ln\frac{I_e(2T)}{I_e(0)}=-2\gamma_s T-\ln\left\{\left[1+3\left(\frac{2T}{2\tau_{tr}}\right)^2\right]\left[3+\left(\frac{2T}{2\tau_{tr}}\right)^2\right]\right\}.$$

[16] P. R. Berman, *Collisions in Atomic Vapors*, Les Houches Lectures, Session XXXVIII, 1982 – New Trends in Atomic Physics, Vol. I, Course 4, edited by G. Grynberg and R. Stora (North-Holland Physics, Amsterdam, 1984); P. R. Berman, J. E. M. Haverkort, and J. P. Woerdman, Phys. Rev. A **34**, 4647 (1986).

[17] S. Chandresekhar, Rev. Mod. Phys. **15**, 1 (1943); in *Selected Papers on Noise and Stochastic Processes*, edited by N. Wax (Dover, New York, 1954). This is a well known, authoritative discussion of Brownian motion and the link between the single-particle Langevin equation and the Fokker-Planck equation for the velocity distribution. The coordinate-velocity phase-space distribution function or propagator is derived on pages 22–29. It is shown to satisfy the Fokker-Planck equation on pages 33–40. The explicit form of the propagator appears on pages 28 and 29, Eqs. (178) and (181)–(183).

[18] For plane waves, which lack a transverse-field distribution, the integral over transverse coordinates in Eqs. (A3) and (A5) is unphysical; $B(T_s)$ is then the peak intensity and reduces to $[\Pi_j G_j(\theta_j)]^2$, where θ_j has been defined in Eq. (9) as the usual pulse area. In this case the signal is measured as the echo intensity or fluence, and the standard echo result is reproduced without transit effects.